Convolutional Neural Network for Tuberculosis Diagnosis: A Review

Dr Santosh Kumar Singh, Assistant Professor

Department of Health & Allied Science, Arka Jain University, Jamshedpur, Jharkhand, India

ABSTRACT: ***Tuberculosis is life-threatening infectious disease that mostly affects the lungs. Small droplets thrown into the air by coughs or sneezes spread tuberculosis germs from one person to the next. The approach for detecting active tuberculosis and latent infection has remained essentially constant throughout the previous few decades. The tuberculin skin test, which employs the purified protein derivative to identify latent infection, is still used today. Researchers developed a deep CNN based on the computer aided diagnosis method for the automated tuberculosis screening in this study. The author used the influence of transfer learning to acquire TB screening results of 0.96, 0.94, and 0.88 in terms of AUC for three real-world datasets based on large-scale chest X-rays. More precise and quick tuberculosis diagnosis is necessary than ever before in the present worldwide tuberculosis pandemic, which includes a significant number of patients infected with the human immunodeficiency virus and growing rates of multidrug-resistant tuberculosis. Deep learning has become the gold standard in the field of machine learning. Deep convolutional brain networks have been shown to be a viable solution for a variety of visual applications, most notably in PC vision. Deep CNN, which considers start to finish preparation from element extraction to gathering without the need for particular has highlight layout, may well be investigated further.***

KEYWORDS: ***Chest X-Rays (CXR), Convolutional Neural Network (CNN), Diagnosis, Human Immunodeficiency Virus Infection (HIV), Tuberculosis (TB).***

1. INTRODUCTION

Tuberculosis is an infection caused by Mycobacterium tuberculosis bacteria that mostly affect the lungs. Tuberculosis may be treated and prevented. Tuberculosis (TB) is transmitted through the air, beginning with one individual but then spreading toward others. The TB germs are transferred high up when persons with lung TB hack, wheeze, or spit. It just takes a handful of these bacteria to get someone sick [1]. A quarter of the people has tuberculosis, which means they are sick but not handicapped, and hence unable to spread the disease. Individuals infected with tuberculosis germs have a 6 to 10% chance of developing the disease all through the course of their lives. Individuals with a weakened immune system, such as those with HIV (Human immunodeficiency infection), malnutrition, diabetes, or who smoke, are more likely to become ill. When a person has active TB, side effects including hacking, night sweats, fever, or weight loss can linger for months or even years. This might lead to treatment delays and the transmission of germs to other people. Patients with dynamic TB can infect an additional 5-15 persons through personal contact over the course of a year. Virtually all HIV-pessimistic TB patients and 45 percent of HIV-positive TB patients would die if they did not seek therapy.

1.1 Most at risk:

Tuberculosis is more common in persons who are in their peak working years. All age groups, however, are at danger. Developing nations account for over 95% of all diseases and fatalities. Active tuberculosis is 18 times more prevalent in HIV-positive individuals (see TB and HIV section below). People with disorders that weaken the immune system are more likely to acquire active tuberculosis. Malnourished people have a threefold increased risk of death. According to the World Health Organization, unhealthiness resulted in 2.2 million new tuberculosis infections. Tobacco and alcohol use both increase the risk of tuberculosis by a factor of 3.4 or 1.6, respectively. 0.73 million new tuberculosis cases were caused by alcohol usage, whereas 0.70 million were caused by smoking [2].

1.2 Global impact of TB:

Tuberculosis (TB) is a highly infectious disease that affects people all over the world. The WHO South-East Asian area (44.0%) had the most new TB cases, following by the WHO African regions (26.0%) for the Who Western Pacific district (26.0%). (20.00 percent). 18% of the total population. The 30 countries with the worst TB problems accounted for 87 percent of all new TB infections. Indonesia, India, the Philippines, India, Nigeria, Pakistan, Bangladesh, and South Africa accounted for 66% of new TB cases.

1.3 Key facts:

1.4 million individuals died of tuberculosis, with 209000 HIV positive persons among them. TB is one of the top ten causes of death in the globe, and the second-leading cause of death due to a single dominating subject matter specialist. An estimated 11 million individuals worldwide would get TB. (TB). There are 5.7 million males, 3.2 million women, and 1.2 million children in the nation. Tuberculosis affects people of all ages and from all walks of life. Tuberculosis, on the other hand, is treated and preventable. Tuberculosis was discovered in 1.2 million children. Adolescence or juvenile TB is sometimes overlooked by health professionals, yet it can be difficult to detect or treat. The 30.0 countries with the worst TB problems accounted for 87.00 percent of all new TB infections. On the overall, India, Indonesia, India, the Philippines, Pakistan, Nigeria, Bangladesh, or South Africa account for 66% of the total, with India leading the pack, followed by Pakistan, Nigeria, Indonesia, India, the Philippines, Bangladesh, and South Africa.

MDR-TB, or multidrug-resistant tuberculosis, is still a clinical and security concern, 206030 persons with multidrug-resistant or rifampicin-resistant TB were discovered or prompted in the world, up 10% from 186884. Tuberculosis is declining at a global rate of roughly 2.00 percent each year, with just a 9 percent drop from 2015. This barely gets us halfway to the End TB Strategy's goal of a 20% reduction in TB cases. Between 2000 to 2015 TB identification or treatment is predicted to have saved 60.00 million lives. The Sustainability Development Goals include a goal of ending the TB epidemic by 2030 as a well-being goal [3].

1.4 Deep convolution neural network (CNN):

CNN is feed forward brain networks that recreates visual open field using a tiled sample. Every convolution operation limit arrangement (also known as a convolution channel) recovers broad visual ideas from the underlying information images, while the configuration of all-encompassing layer boundaries sorts the recovered visual spotlights into target classes[4]. Lower convolution layers separate low-level attributes, such as target object sub-parts, from crude information pictures, while higher convolution layers extricate significant level visual ideas, such as target object sub-parts, in a progressive design, with the low convolution layer separating lower-level attributes, such as target object sub-parts, and displayed in Table 1 [5].

Table 1: In this study, architecture of the deeps convolutional neural networks was used [5]

Layer #*	Type (activation)	Input Shape **	Filter Size ***-Stride
M1	Max Pool	(1, 500, 500)	(96, 1, 11, 11) - 4
C1	Convolution (ReLU)		(3, 3) - 2
M2	Max Pool	(96, 61, 61)	(256, 96, 5, 5) - 1
C2	Convolution (ReLU)		(3, 3) -2
M3	Convolution (ReLU)	(256, 30, 30)	(384, 256, 3, 3) - 1
C3	Convolution (ReLU)	(384, 30, 30)	(384, 384, 3, 3) - 1
M4	Max Pool	(384, 30, 30)	(256, 384, 3, 3) - 1
C4	Convolution (ReLU)	(256, 15, 15)	(3, 3) - 2
M5	Max Pool	(384, 30, 30)	(256, 256, 3, 3) - 1
C5	Convolution (ReLU)		(3, 3) - 2
M6	Max Pool	(256, 15, 15)	(2048, 12544)
C6	Convolution (ReLU)		
F7	Fully Connected (ReLU)	(256*7*7)	(2048, 2048)
D7	Dropout		
F8	Fully Connected (ReLU)	(2048)	(2, 2048)
D8	Dropout		

i. Layers = C ("Convolution"), M ("Max Pool"), F ("Fully Connected"), D ("Decomposition")

ii. Convolution (number of channel, image height, image width,), Completely Connected (number of flattened node) Input Shape

Filters Size = Max Pool ("kernel height, kernel width"), Entirely Connected ("number of filters, number of channels, kernel height, kernel width"), Convolution ("amount of filters, number of connections, kernel height, kernel width") ("number of output nodes, number of inputs node").

CNN does not require extensive human component design in light of space explicit talent since it develops the optimal discriminative aspects as suggested by the target aim (e.g., TB characterisation) from available information[6]. For example, in more established TB screening formulas, the morphological characteristics of distinct damage instances should be defined first. We built our deep CNN for this study using a famous CNN technique named alexnet, which has been optimized for the general picture recognition. People included an additional convolution layer for include extraction since the information CXR aim is often large when compared to standard item recognition tasks. The data size in this study is 520520 bytes, however the images used are 256256 bytes. Because there were less prepared photos and groups, the number of hidden hubs in entirely associated layers (for example, classifier) was reduced. Table 1 summarizes our in-depth CNN engineering. Because we arbitrarily slice 520520 photographs to 500500 for dataset growth, the information size of the primary convolution layer C1 is 500500.

2. LITERATURE REVIEW

A. Ainley and O. M. Kon, the authors observed that VGG(Visual Geometry Group) Net outperformed Alexnet on the Montgomery and Apoorva CXR (Chest X-Rays) datasets owing to VGG(Visual Geometry Group) Net's deeper network. VGGNet had an accuracy of 81.6 percent, whereas Alexnet had an accuracy of 80.4 percent. The authors come to the conclusion that using a larger dataset in the experiment increases performance accuracy[7].

Y. Sun, to train their model using unbalanced, less categorized X-ray images, the researchers utilized cross-validation with sample shuffling. The experiment used the Peruvian TB datasets, which comprised a total of 4701 image samples, 4248 of which were tagged as abnormal, including six tuberculosis symptoms, and 453 of which were marked as normal[8].

U. K. Lopes and J. F. Valiati, to train their model using unbalanced, less categorized X-ray images, the researchers utilized cross-validation with sample shuffling. The experiment used the Peruvian TB datasets, which comprised a total of 4701 image samples, 4248 of which were tagged as abnormal, including six tuberculosis symptoms, and 453 of which were marked as normal[9].

Y. Tian, as demonstrated by the linked research, more work is needed to battle TB epidemics, which has remained one of top causes of mortality. As a result, we've shown that detecting and categorizing CXR for the tuberculosis manifestation has a higher accuracy of performance validation. Tuberculosis, a lethal infectious respiratory disease, seems to have been a leading cause of death worldwide for decades. The chest X-ray (CXR) became the most commonly used medical imaging technology for identifying tuberculosis due to its simplicity, efficiency, or cost-effectiveness. The use of automatic CXRs for tb identification and detection of potentially TB-positive regions is expected to significantly enhance TB diagnostic quality [10].

3. DISCUSSION

The next subsections go into the datasets and techniques used to develop the TB detection CAD system. In actuality, having a big amount of data to train deep networks is uncommon. To deal with this challenge, pre-prepared CNN model based on a huge scope dataset, including the Image Net dataset with 1.3 million photos and 1000 classes, are typically used. The pre-prepared models give the essential criteria for organizing loads. Deep CNN can be adequately prepared even with datasets of extremely restricted scope because to such explicit initial loads. This strategy is referred to as "move learning." Regrettably, this has little bearing on clinical images, as their characteristics are strikingly different from those of standard images [11]. We created the CNN using the preparation and approval datasets and arbitrarily imposed loads in all levels using the methodology shown in Table 1. We discovered that the number of images provided is insufficient for thorough organization planning (see Figure 2). Overall, in a high-layered boundary space, acquiring properly prepared boundaries (network

loads) for the aim goal job (e.g., cross-entropy suffering exhibiting characterization botches) is difficult (33,317,827-layered boundary space in this engineering). Preparing misfortune reduces progressively with unsuitably focused approval precision execution, as seen in (cost bends labelled "Preparing misfortune w/o TL" and "Acceptance exactness w/o TL"). To lessen the influence of the arbitrary division, the trials were performed multiple times, and the relevant datasets were given the designations Dataset 1, 2, or 3. They utilized convolution bounds that had already been established (channels from the first or second convolutions operation in profound CNN prepared on the Image Net characterization dataset) for underlying upsides of boundaries in low convolution layers because lower convolution layers (C1 and C2) extricate low-level elements like edges and bends from the information pictures (C1 and C2). The channels of the principal convolution layer C1 that were relocated from the pre-prepared model are shown in Figure 1. Because the information images used for preparation in their development comprise RGB variety components, the initial channels have a channel size of three[12]. We simply provide channel values together with channel characteristics to our CNN for preparation using single-channel CXRs. They're useful for separating lower level data from the input images, like as edges or directions (see Figure 1).

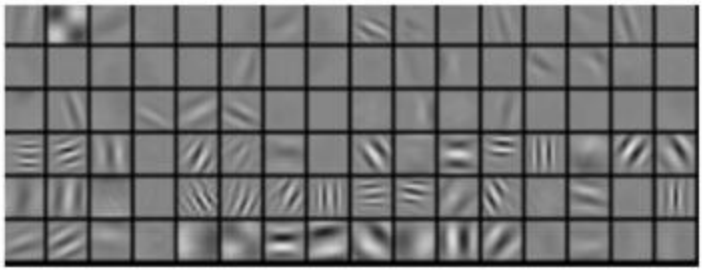

Figure 1: The initial filters are presented in first convolution layers C1. C1 has a total of 96 filter, each measuring 11*11 pixels.

As shown in Table 2, we used three CXR datasets in this study: the KIT, MC, and Apoorva sets. All of CXRs used in this investigation were de-identified by linked images sources.

Table 2: Illustrate the Dataset descriptions utilized in this investigation.

Dataset Name	Description
KIT	10,848 DICOM data, consisting of 7020 normal and 3828 abnormal (TB) cases, from the Korean Institute of Tuberculosis (KIT) under Korean National Tuberculosis Association (KNTA), South Korea
MC	138 PNG data, consisting of 80 normal and 58 abnormal (TB) cases, from National Library of Medicine, National Institute of Health, Bethesda, MD, USA
Apoorva	662 PNG data consisting of 326 normal and 336 abnormal (TB) cases, from Approva no.3 People's Hospital, Medical College, GandhiNagar, India.

The KIT set (10,948 CXRs) was randomly distributed into training (70.00%), validation (15.00%), or test (15.00%) sets to check the screening performances of deeps CNN. The deep CNN is trained using the training data set, the validation data is being used to assess the trained deep CNN's validity, and the test dataset has been used to quantify screened performance. To verify that the data was treated equally, this random split was repeated three times ("i.e. 3-fold cross validation"). To demonstrate how effectively the KIT-prepared deep CNN worked across datasets, the MC or Apoorva datasets were employed. The piles of each layer started with a zero-mean Gaussian appropriations with standard deviation of 0.01, and initial inclinations were set to 0. Each layer's piles started with a zero-mean Gaussian flow with such a standard deviation of 0.01, and beginning inclinations were set to 0. All heaps in each layer were started from a zero-mean Gaussian dispersion with a standard deviation of 0.01, and beginning inclinations were set to 0 except the first and second convolution layers C1 or C2, whose heaps were transferred from the pre-arranged model. We started with a learning rate of 0.01 and, like clockwork, reduced it by a factor of two. For move learning of lower level channels, you put up a fundamental learning tempo of 0.001 for the relevant layers, such as C1 or C2. The connection was established using a stochastic inclination drop with an energy of 0.9 and a reduced pack size of 64. By separating endorsement precision, a

framework search was used to separate the weight decay limit. Every one of the tests in this evaluation was driven by Caffe, an openly available deep learning stage[13]. The influence of lower level channel motion learning is seen in Figure 2. As a consequence of the influence of move learning, arrangement expenses condense even faster with higher recommendation exactness ("for example, better neighborhood minima"), as seen in the graph. Despite the fact that CXRs or nonexclusive images share lower level visual concept ("example edges, bends"), move learning of lower pre-prepared channels is strong in light of the fact that important level ideas are semantically distinct ("e.g., portions of articles"). Stochastic slope drop with an energy of 0.9 and a scaled down bunch size of 64 was used to prepare the organization. A matrix search was used to differentiate the weight rot boundary by contrasting approval exactness. Caffe, a freely available deep learning stage, was used to drive each of the testing in this study. Figure 2 depicts the influence of lower level channel move learning).

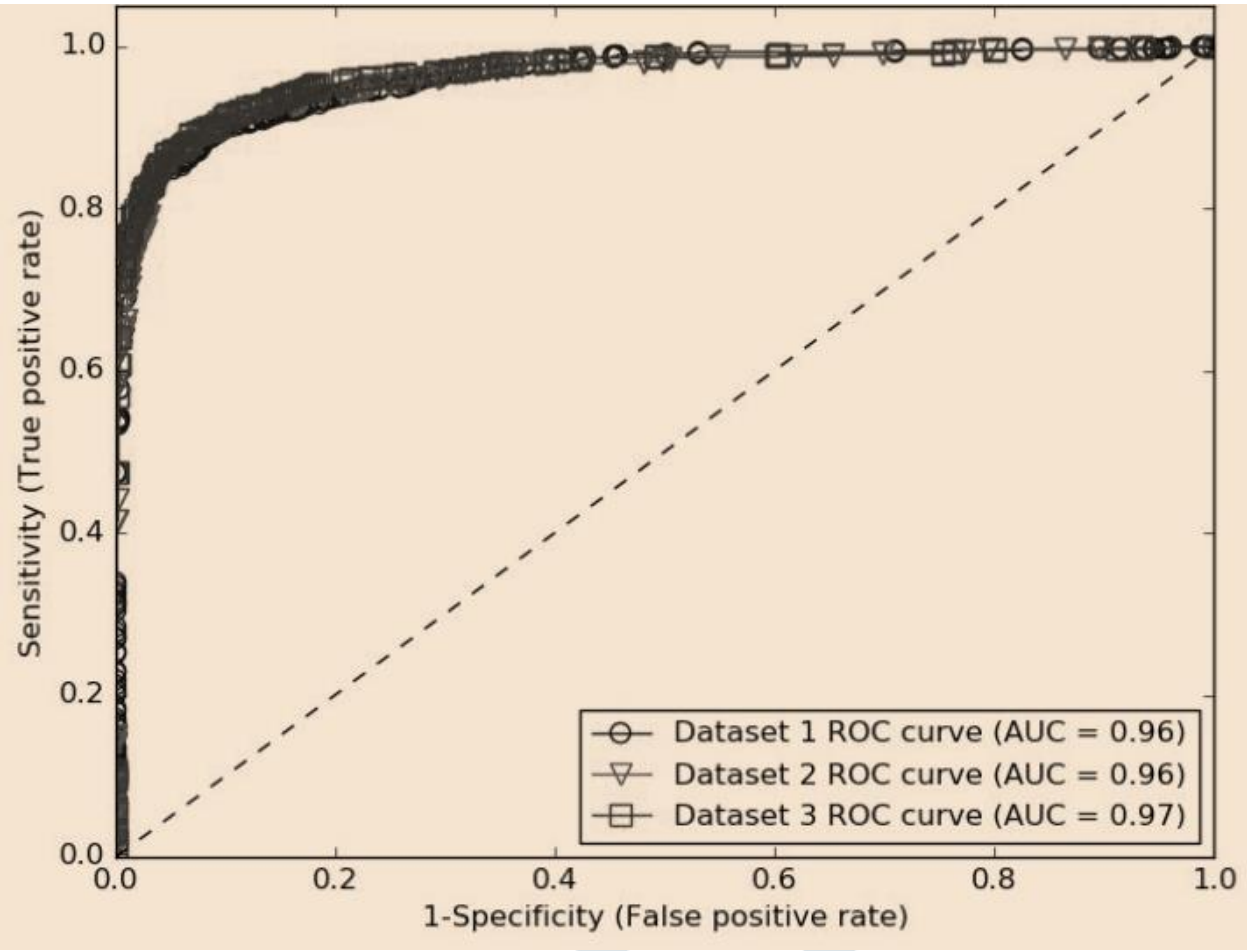

Figure 2: AUC values for three distinct datasets on ROC curves[4]**.**

Because the quantity of pictures required for training is often restricted in the medical field, this result is extremely significant. The ROC curves of three repeatable testing using area-under-curve are shown in Figure 2. (AUC). As you can see from the table below (Table 3) Figure shows that the ROC curves in all three studies were comparable, with such a higher AUC (0.965 in average).

Table 3: Comparison of deep CNN performances either with or without domain adaptation [8]

	Without Transfer Learning				With Transfer Learning			
	AUC	Accuracy	AP (pos)	AP (neg)	AUC	Accuracy	AP (pos)	AP (neg)
Dataset 1	0.884	0.783	0.750	0.894	0.973	0.912	0.961	0.984
Dataset 2	0.838	0.798	0.769	0.889	0.973	0.915	0.960	0.989
Dataset 3	0.796	0.768	0.731	0.878	0.977	0.914	0.967	0.978
Average	0.826	0.784	0.753	0.887	0.926	0.913	0.953	0.987

3.1 Cross-Dataset Performance Analysis:

Additional experiments were performed using the MC and Apoorva datasets to confirm the cross dataset findings of CNN trained with the KIT dataset. Table 4 compares the proposed deep CNN's efficiency to that of earlier studies on the identical test sets. This isn't a direct comparison of performance; rather, it's a general estimate of our deep CNN's screening capabilities. Dataset k was used to train the deeper CNN Net k. To create ensemble data, humans averaged the class probabilities from Net 1, 2, or 3. Figure 3 illustrates the ROC curves [9].

Table 4:Illustrate the Screening Performance for MC or Apoorva Sets[9]

	Without Transfer Learning				With Transfer Learning			
	AUC	Accuracy	AP (pos)	AP (neg)	AUC	Accuracy	AP (pos)	AP (neg)
Net 1	0.887	0.663	0.869	0.894	0.927	0.832	0.932	0.894
Net 2	0.875	0.846	0.880	0.870	0.928	0.835	0.934	0.909
Net 3	0.756	0.603	0.879	0.846	0.920	0.831	0.934	0.908
Ensemble	0.826	0.784	0.889	0.889	0.926	0.838	0.940	0.917
TMI 14	0.876	0.884	-	-	0.910	0.834	-	-

Because these datasets have various modalities, such as different countries, different X-ray apparatus for the image capturing, and so on, screening results for the MC or Apoorva sets are slightly lesser than the KIT set. Because of the different modalities, the output ordinary least square from the MC or Apoorva sets is moved. The best accuracies for the MC but also Apoorva sets are 0.877 and 0.847, respectively, at probability thresholds of 0.8 and 0.6. These problems can be addressed by training the deep CNN with new datasets that span a wider variety of modalities. Table 4 shows that the trained network recognizes the Apoorva set better than the MC set. We determined that CXR's fundamental image properties are to fault. The KIT collection has nearly all CXRs from Digital Radiography, but the MC and Apoorva collections have pictures from both Computed and Digital Radiography. Given the vast variations in datasets, our CNN performs well in terms of filtering [7].

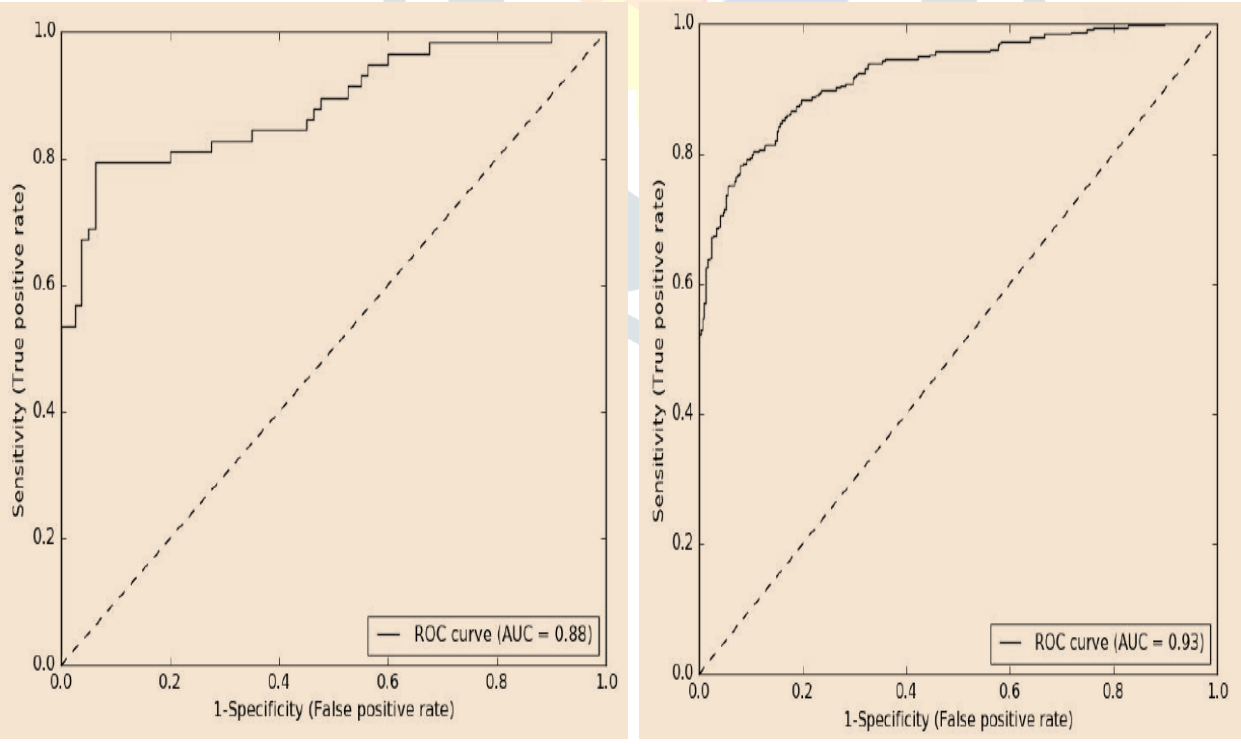

Figure 3. The Apoorva set (left) or the MC put are bent by ROC (right). Each AUC esteem is recorded in the tale. [7]**.**

Machine learning is a field of artificial intelligence wherein the computer learn to understand existing data associations in order to do tasks without being explicitly instructed. We use supervised DCNNs in this work, a sort of deep learning with numerous hidden layers that has been shown to be quite excellent at classifying photos.

The computer was supervised because it was trained on a large number of pre-labeled samples. One of the advantages of deep learning is its ability to thrive with high-dimensional data, such as images, which may be represented at several levels. DCNNs might be represented using pixel intensity values, edges, or blobs at lower levels; pieces of things at different stages of development; and the full object at higher levels.

DCNNs that had been pre-trained using daily photos from Image Net outperformed untrained networks in our investigation, which is in line with earlier research (Table 3, Fig 2). Transfer learning is the term for this phenomenon. Although it may not appear at first that utilizing pre-trained networks with non-medical photographs can aid with medical image classification, there are characteristics in all images that are comparable, such as the edges and blobs that make up the neural network's first layers. After using the pre-trained network to medical images, the fully connected layers were set to different initial conditions of weights so that they might retrain from either the medical images given.

Rotated images were added to the dataset, and image contrast was improved via Contrast Limited Adaptive Histogram Equalization (Table 3, Figure 2). When the number of variables fed to the neural network is increased, the DCNN's generalization and performance improve. More prospective research on the use of DCNNs in clinical practice for tuberculosis assessment in the lungs, particularly in TB-endemic areas, would be beneficial. It would be intriguing to see how more training examples or various ways to augmentation affect accuracy. To directly analyze the influence of Digital Imaging and Communications in Medicine files as well as other deep neural network topologies, more research is required. Finally, with an AUC of 0.99, deep learning using DCNNs can properly diagnose TB during chest radiography. When the DCNNs couldn't agree, a radiologist-assisted technique with a sensitivity of 97% and a specificity of 100% improved accuracy even further.

4. CONCLUSION

The author proposes a sophisticated CNN-based robotized TB screening approach in this paper. The first TB screening framework based on deep CNNs or prepared with CXRs has been developed. The recommended technique for TB screening does not require physically manufactured highlights since CNN develops the appropriate discriminative highlights based on the objective point from available information. Move acquiring from lower convolution layers of pre-prepared organizations has also been shown to solve problems like processing high-goal clinical images and preparing large boundaries with few shots. Computational experiments using 3 real world datasets: MC, KIT, or Apoorva indicate that proposed framework performs well in terms of screening for a variety of exhibition indicators. Separating this study, we developed a comprehensive CNN-based PC assisted determination (CAD) framework for robotized TB. Due to the large scope of the chest X-beams, we relied on the power of movement to attain our goals. In terms of AUC, Tuberculosis screening performances was 0.96, 0.94, or 0.88 for three real-world datasets.

REFERENCES

[1] Y. Cao *et al.*, “Improving Tuberculosis Diagnostics Using Deep Learning and Mobile Health Technologies among Resource-Poor and Marginalized Communities,” 2016. doi: 10.1109/CHASE.2016.18.

[2] M. Murray and D. Alland, “Methodological problems in the molecular epidemiology of tuberculosis,” *Am. J. Epidemiol.*, 2002, doi: 10.1093/aje/155.6.565.

[3] P. Vulliémoz and G. Favez, “Exploration hépatique chez le tuberculeux pulmonaire par les méthodes enzymatiques. Recherche d’un éventual effet hépato-toxique des médicaments antibacillaires,” *Respiration*, 1964, doi: 10.1159/000192345.

[4] S. Hwang, H.-E. Kim, J. Jeong, and H.-J. Kim, “A novel approach for tuberculosis screening based on deep convolutional neural networks,” 2016. doi: 10.1117/12.2216198.

[5] S. Narayanan, “Molecular epidemiology of tuberculosis,” *Indian Journal of Medical Research*. 2004. doi: 10.1183/09031936.02.00400702.

[6] M. M. Mesfin *et al.*, “Cost implications of delays to tuberculosis diagnosis among pulmonary tuberculosis patients in Ethiopia,” *BMC Public Health*, 2010, doi: 10.1186/1471-2458-10-173.

[7] R. Grob, “A house on fire: Newborn screening, parents’ advocacy, and the discourse of urgency,” in *Patients as Policy Actors*, 2011.

[8] E. Horvitz and R. White, “How web search data might help diagnose serious illness earlier,” *Journal of Oncology Practice*, 2016.

[9] R. Gokhale, A. Acosta, and H. Shafi, “1764: SURVIVING MARDI GRAS IN THE INTENSIVE CARE UNIT,” *Crit. Care Med.*, 2016, doi: 10.1097/01.ccm.0000510437.34933.67.

[10] H. Erdem, A. K. Uzunlar, Ü. Yildirim, H. Yaman, L. Aydin, and C. Şahiner, “Extrapulmonary tuberculosis,” *Duzce Med. J.*, 2012.

[11] G. F. Mgode *et al.*, “Mycobacterium tuberculosis volatiles for diagnosis of tuberculosis by Cricetomys rats,” *Tuberculosis*, 2012, doi: 10.1016/j.tube.2012.07.006.

[12] V. Meyssonnier *et al.*, "Factors associated with delayed tuberculosis diagnosis in China," *Eur. J. Public Health*, 2013, doi: 10.1093/eurpub/cks037.

[13] C. Lange and T. Mori, "Advances in the diagnosis of tuberculosis," *Respirology*. 2010. doi: 10.1111/j.1440-1843.2009.01692.x.